To cite this version: Sharma, Amit and Julcour-Lebigue, Carine and Kelkar, Ashutosh A. and Deshpande, Raj M. and Delmas, Henri (2009) Mass Transfer and Solubility of CO and H2 in Ionic Liquid. Case of [Bmim][PF6] with Gas-Inducing Stirrer Reactor. *Industrial & Engineering Chemistry Research*, vol. 48 (n° 8). pp. 4075-4082. ISSN 0888-5885

Mass Transfer and Solubility of CO and H$_2$ in Ionic Liquid. Case of [Bmim][PF$_6$] with Gas-Inducing Stirrer Reactor

Amit Sharma,[†] Carine Julcour,*,[†] Ashutosh A. Kelkar,[‡] Raj M. Deshpande,[‡] and Henri Delmas[†]

Université de Toulouse, Laboratoire de Génie Chimique, Ecole Nationale Supérieure des Ingénieurs en Arts Chimiques et Technologiques (ENSIACET), Toulouse, France, and Chemical Engineering Division, National Chemical Laboratory, Pune 411008, India

Since the past decade, ionic liquids have gained significant importance as alternative solvents for catalysis applications. Many of the reactions evaluated in ionic liquids employ gases as substrates, and therefore it is important to know their solubility and mass transfer characteristics. This work reports for the first time both the solubility and volumetric gas−liquid mass transfer coefficient k_La for hydrogen and carbon monoxide in 1-*n*-butyl-3-methylimidazolium hexafluorophosphate ([Bmim][PF$_6$]) at three temperatures (293, 323, and 373 K) in relevance to hydroformylation reaction. The experimental data on the volumetric gas−liquid mass transfer coefficient are described by a dimensionless correlation for the bench-scale stirred tanks with gas-inducing impeller. k_La values have also been evaluated for different [Bmim][PF$_6$]−decane emulsions at 373 K.

1. Introduction

Among many applications as solvents, ionic liquids are being viewed as alternative solvents to water, particularly in cases where water can interact with transition metal catalysts or substrates have very low solubility in water.[1−3] This has led to research activities mainly on the development of new catalyst/ solvent systems for various reactions. However, there are limited reports addressing reaction engineering aspects: intrinsic kinetics—needing the concentration of the dissolved gases and organic substrates in the ionic catalytic phase—and evaluation of mass transfer limitations in such highly viscous media.

The aim of the joint NCL Pune and LGC Toulouse project is to approach these questions related to quantitative engineering of gas−liquid−liquid reactions with ionic liquids as it was yet investigated in usual aqueous biphasic catalysis at LGC by Hablot et al.,[4] Purwanto and Delmas,[5] Purwanto et al.,[6] Desphande et al.,[7] Lekhal et al.,[8] and Jauregui-Haza et al.[9]

There are recent reports on gas solubility in ionic liquids;[10,11] however, there are no investigations on the gas−liquid mass transfer in these media. This work especially deals with solubility and mass transfer of H$_2$ and CO in 1-*n*-butyl-3-methylimidazolium hexafluorophosphate ([Bmim][PF$_6$]), the ionic liquid selected for biphasic hydroformylation kinetics. Solubility and mass transfer rates have been measured by pressure variations in a gas self-induced reactor.

2. State of the Art: Gas Solubility and Mass Transfer in Ionic Liquids

Over a decade ionic liquids (ILs) have sparked an increased collective interest of chemists and technologists for reaction chemistry, including catalytic reactions. The bulk of ionic liquid research has been focused on the use of ILs as solvents for a variety of reactions and only recently on their physicochemical properties.

Multiphase reaction systems are frequently encountered in chemical reaction engineering practice, and there are several industrially important applications, such as hydrogenation, hydroformylation, alkylation, ozonolysis, oxidation with molecular oxygen, ammonolysis, addition halogenation, etc., where it is desirable to have practically complete utilization of the solute gas. A gas-inducing stirred reactor is likely to provide better gas−liquid contact than other reactors with possibly lower power consumption.[12] However, a clear understanding of gas solubility and mass transfer is important in understanding the reaction engineering aspects of any reaction.

Ionic liquids offer new opportunities for the development of improved biphasic systems.

In aqueous biphasic systems low reaction rates are usually obtained because of phase transfer limitations caused by low substrate solubility in the catalyst phase. On the other hand, ionic liquids are good solvents for a wide range of both organic and inorganic species without undesirable interactions with the metal center.

Thus, biphasic hydroformylation of higher olefins using rhodium−phosphine complexes in room-temperature ionic liquids (RTILs), like [Bmim][PF$_6$] or [Bmim][BF$_4$], has proved to be a very attractive alternative to current aqueous system.[1]

Biphasic systems using ionic liquids to retain the homogeneous catalyst result in additional mass transfer steps but enable desired catalyst recycling via simple decantation. In particular, the modeling of reaction under such mass transfer limitations will require the knowledge of both gas−liquid equilibria and mass transfer coefficients (k_La). There are no available results on mass transfer effects in ionic liquid based biphasic catalysis. However, there are several reports on solubility of gases in ionic liquids.[10,11,13−17] Solubility of different gases (carbon dioxide, ethylene, ethane, methane, argon, oxygen, carbon monoxide, hydrogen, and nitrogen) in [Bmim] [PF$_6$] has been measured by Anthony et al.,[11] but they have reported that the solubility of carbon monoxide, hydrogen, and nitrogen was below the detection limit of their apparatus. Kumelan et al. have given values of Henry's constant in [Bmim][PF$_6$] for carbon monoxide from 293 to 373 K[15] and hydrogen from 313 to 373 K.[16] The hydrogen solubility was found to increase with increase in temperature, whereas no significant temperature dependence was observed for CO solubility. Conversely Jacquemin et al.[17] have observed a maximum for hydrogen solubility in [Bmim][PF$_6$]

* To whom correspondence should be addressed. Tel.: 33 5 34 61 52 40. Fax: 33 5 34 61 52 53. E-mail: carine.julcour@ensiacet.fr.

[†] LGC, ENSIACET.
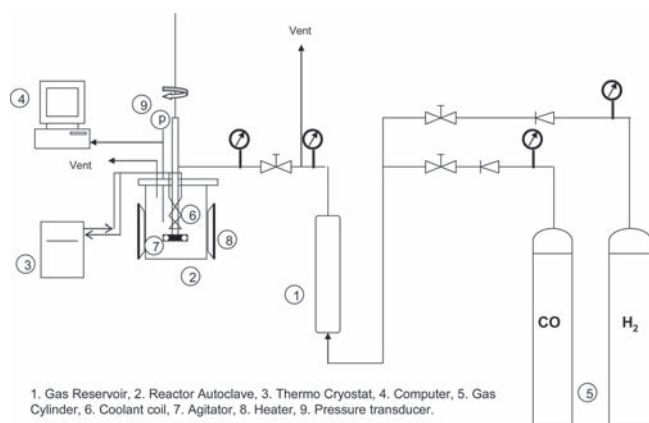
[‡] National Chemical Laboratory.

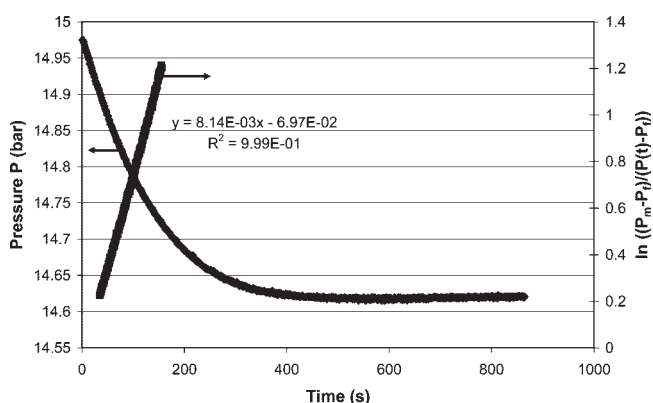**Figure 1.** Schematic diagram of the experimental setup.

Figure 2. Graphical representation of eq 1 for the determination of gas−liquid mass transfer coefficient (H$_2$, 1500 rpm, 20 °C).

Figure 3. Solubility of H$_2$ (a) and CO (b) in [Bmim][PF$_6$] as a function of (equilibrium) pressure at 293 (◆), 323 (gray filled square), and 373 K (△).

around 310 K. The comparison of all data provided by those research groups, who have used different techniques and pressure ranges, exhibits a large scattering of gas solubility values for these low-soluble gases (with deviations up to nearly 200%). Thus, there is a necessity for the development of a robust and high-precision technique to evaluate thermodynamic properties.

In the present article, solubility and mass transfer coefficient of carbon monoxide and hydrogen are reported in [Bmim][PF$_6$]. $k_L a$ values have also been evaluated for [Bmim][PF$_6$]−decane mixtures, using different ratios of the two phases, in order to mimic biphasic reaction media. Measurements have been carried out in an autoclave reactor equipped with a self-gas-inducing agitator.

3. Experimental Section

3.1. Materials. [Bmim][PF$_6$] was obtained from Solvionic with a purity of 99%. The specification for water content is <0.1% (measured at 0.03% according to Karl Fisher titration) and for halide content <0.005%. Thermogravimetry analysis (performed at 150 °C) shows about 0.15% of volatile com-
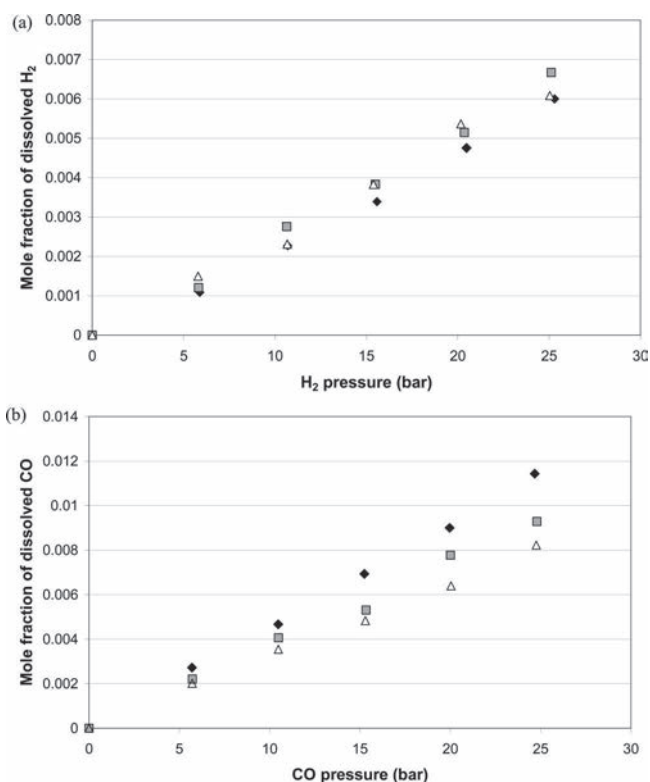
pounds. From headspace gas chromatography/mass spectrometry (GC/MS) analysis, bromobutane (used for IL synthesis) is found as the major volatile impurity.

Decane, 99+ % purity, was supplied by Sigma-Aldrich. Carbon monoxide and hydrogen were purchased from Linde gas s.a.

3.2. Experimental Setup. The schematic diagram of the experimental setup is shown in Figure 1. A 650 mL high-pressure autoclave (flat bottom, internal diameter $d_R = 8 \times 10^{-2}$ m) made of Hastelloy C276 was used for the measurements. The reactor was equipped with two symmetrical baffles (W/d_R = 0.049) and a six-bladed gas-inducing stirrer ($d_{st} = 3.2 \times 10^{-2}$ m) with a variable speed up to 2000 rpm. The stirrer was mounted on a hollow shaft, with holes above the liquid surface.

When the gas-inducing impeller is rotating, the pressure behind the blades is reduced. Above a critical speed the gas is sucked through the holes of the hollow shaft to the holes in the impeller and dispersed into the liquid in small bubbles.

The liquid temperature, measured with a thermocouple, was set using an external heating jacket controlled by a PID. A high-precision pressure transducer (Keller PR33X, uncertainty of less than 0.015 bar) was used to measure pressure variations. Sensitivity of pressure gauges was increased once the pressure operation zone was selected. As only pressure differences were

Table 1. Physical Properties of [Bmim][PF$_6$] Measured between 293 and 373 K^a

temp (K)	density ρ (kg/m^3)	viscosity μ (Pa·s)	surface tension σ (10^{-3} N/m)
293	1371 ± 1 (1368 (298 K)^b, 1360 (298 K)^c)	0.35 ± 0.02 (0.264^d, 0.286^e)	45.8 ± 0.05 (47^b, 48.8 (298 K)^c)
313	1354 ± 1 (1350^b)	0.12 ± 0.01 (0.107^d, 0.094^e)	43.1 ± 0.1^f
323	1345 ± 1 (1339^b)		41.9 ± 0.1^g
333	1337 ± 1	0.055 ± 0.003 (0.049^d, 0.040^e)	
353		0.030 ± 0.001 (0.024^d)	
368		0.021 ± 0.001 (0.015^d)	

^{a} Values in parentheses are literature data. ^{b} Ref 22. ^{c} Ref 23. ^{d} Ref 24. ^{e} Ref 25. ^{f} At 315 K. ^{g} At 320 K.

Table 2. Diffusion Coefficients of H_2 and CO in [Bmim][PF$_6$], According to Morgan et al. (Ref 26)

temp (K)	diffusion coefficient of H_2 (10^{-10} m^2/s)	diffusion coefficient of CO (10^{-10} m^2/s)
293	2.2	1.8
323	5.7	4.7
373	12.9	10.5

Table 3. Henry's Constants (bar) for H_2 and CO in [Bmim][PF$_6$]

temp (K)	Henry's constant H_{H2} (bar)	Henry's constant H_{CO} (bar)
293	$(4.35 \pm 0.12) \times 10^3$	$(2.19 \pm 0.04) \times 10^3$
323	$(3.89 \pm 0.10) \times 10^3$	$(2.66 \pm 0.06) \times 10^3$
373	$(4.00 \pm 0.09) \times 10^3$	$(3.06 \pm 0.06) \times 10^3$

used, it could be considered that uncertainty was limited to the signal noise at constant pressure, i.e., 0.005 bar. Temperature was measured at ± 0.1 °C, whereas temperature control was achieved within ± 0.5 °C. Both temperature and pressure of the reactor were recorded online on a computer at a rate of 1−5 Hz.

3.3. Theoretical Background for the Experiments. The experimental technique used to measure the solubility and hence Henry's constant involved batch absorption of a single gas at a given temperature and pressure and measuring of the total gas pressure variation corresponding to the dissolved gas amount in equilibrium with final pressure. Pressures up to 25 bar were used to ensure accuracy of pressure variation measurement.

Moreover in order to determine the gas−liquid mass transfer coefficient k_La, the dynamics of the pressure variation of the gas phase was recorded as the absorption proceeded. This technique was previously described[18−20] and known as the dynamic pressure step method. After the desired liquid temperature was reached, the reactor headspace was flushed with the gas solute and the liquid was saturated at low pressure ($P_0 = P_{atm}$). Then the stirring was stopped and the gas solute pressure was rapidly increased in the reactor (to P_m). At $t = t_0$, the stirrer was started again and the pressure was recorded as a function of time until it remained constant (new equilibrium pressure P_f). Integration between $t = t_0$ ($P = P_m$) and t of the mass balances in gas and liquid phases (perfectly stirred) leads to

$$\ln\left(\frac{P_m - P_f}{P(t) - P_f}\right) = \left(\frac{P_m - P_0}{P_f - P_0}\right) k_L a (t - t_0) \qquad (1)$$

A typical plot is shown in Figure 2: k_La value can be determined from the slope of the line.[21] The main question about this technique concerns the part of the pressure curve to be used as the stirrer speed cannot be instantaneously varied from zero to the desired speed. The best choice is to select the portion which best fits the exponential pressure variation. It corresponds to the linear variation of the logarithmic pressure difference ratio, from about 20% to 70% of the total pressure variation.

4. Results and Discussion

4.1. Physical Properties of [Bmim][PF$_6$]. All relevant physical properties of [Bmim][PF$_6$] except diffusivity were measured between 293 and 373 K and are given in Table 1. Those data are found in good agreement with previously published values.

The density of [Bmim][PF$_6$] was determined using an oscillating U-tube densimeter (Anton Paar DMA 38) and was well described as a linearly decreasing function of temperature:

$$\rho(\text{kg/m}^3) = 1621.3 - 0.85T \qquad (2)$$

where temperature T is in Kelvin.

Rheometer measurements (TA Instruments CSL2 500) showed that [Bmim][PF$_6$] has a Newtonian behavior. Its viscosity was measured at various temperatures, and data regression gave the following dependence with temperature:

$$\mu(\text{Pa·s}) = \exp\left(-14.945 + \frac{4042.4}{T}\right) \quad (T \text{ in K}) \qquad (3)$$

The surface tension of [Bmim][PF$_6$] was experimentally determined using Wilhelmy plate method (GBX 3S tensiometer) and could be expressed as

$$\sigma(\text{N/m}) = (85.48 - 0.135T) \times 10^{-3} \quad (T \text{ in K}) \qquad (4)$$

The diffusivity of hydrogen and carbon monoxide in [Bmim][PF$_6$] was estimated using the correlation compiled by Morgan et al.[26] The authors have measured the diffusivity of carbon dioxide, ethylene, propylene, 1-butene, and 1,3-butadiene in six different ionic liquids, including [Bmim][PF$_6$], at 30 °C using a lag-time technique. They have found diffusivity values much greater than those predicted by Stokes−Einstein or Wilke−Chang equations (after fitting the solvent association coefficient to an unusual value of 0.15). So they have proposed the following correlation which accounts for the liquid molar volume ($\overline{V}_1$ in cm^3/mol) of the solute 1 at its atmospheric boiling point, the viscosity (in cP) and density (in g/mL) of imidazolium ionic liquid 2:

$$D = 3.7 \times 10^{-7} \frac{1}{\mu_2^{0.59 \pm 0.02} \overline{V}_1^{(1.0 \pm 0.07)} \rho_2^{2.0 \pm 0.1}} \qquad (5)$$

with diffusivity D in m^2/s.

This correlation was used without further modification to estimate diffusivities in the investigated range of temperatures (293−373 K), and the corresponding values are reported in Table 2.

4.2. Solubility Studies. The absorption of H_2 and CO into [Bmim][PF$_6$] was measured at three different temperatures—293, 323 and 373 K—using a high-precision pressure sensor. Before performing the solubility experiments, the free reactor volume (subtracting all fittings and stirrer volumes) was determined precisely by filling it with nitrogen from a known volume ballast and measuring pressure variations. The value obtained (615 ± 3 mL) was also verified by measuring the known Henry's constant for the N_2−water system at room temperature. Several experiments were performed with H_2−[Bmim][PF$_6$] and CO−[Bmim][PF$_6$] systems to check for the repeatability of the results (estimated at less than 5%). For all the experiments, the reactor was filled with 300 mL of [Bmim][PF$_6$].

Figure 3, parts a and b, shows the experimental data plotted as the mole fraction of the gas dissolved in the liquid phase versus the absolute pressure of the gas at different temperatures. As can be seen, the trend followed is linear, suggesting that Henry's law is applicable. The results of solubility in terms of Henry's constants (in bar) are listed in Table 3.

From the variations of Henry's constants as a function of temperature, the enthalpy of solvation of H_2 can be roughly estimated at 3.0 kJ/mol between 293 and 323 K and −0.60 kJ/mol between 323 and 373 K, whereas for CO a constant value of −3.8 kJ/mol can be considered on the whole temperature range.

In accordance with previous studies,[15−17] solubility of CO was found larger than that of H_2 in the investigated range of temperatures. The trend as a function of temperature is consistent with that observed by Jacquemin et al.[17] (decrease of CO
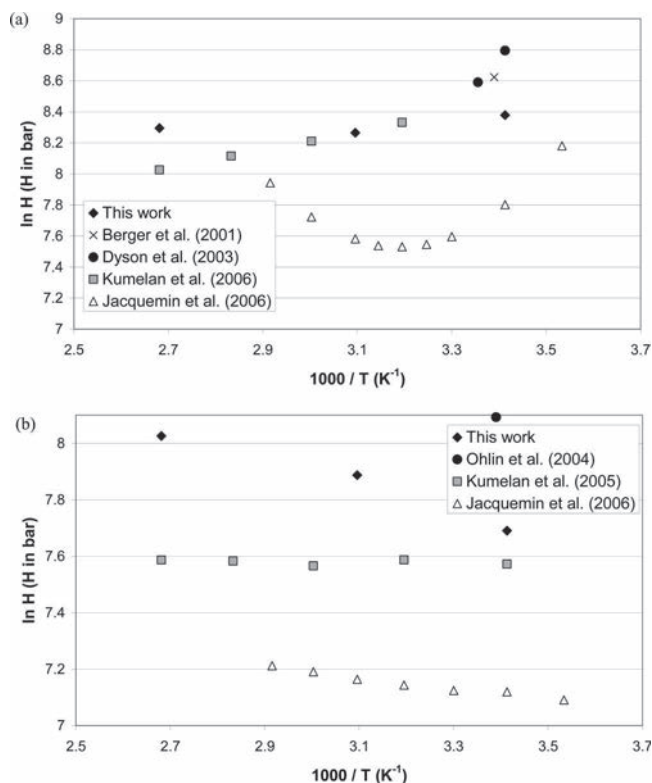
Figure 4. Ln H (Henry's constant) vs the inverse of temperature (K) for H_2 (a) and CO (b) in [Bmim][PF$_6$].

solubility with increasing temperature, maximum of solubility for H_2 in the investigated range); however, the temperature effect is much more significant for CO than H_2.

As shown in Figure 4, the values measured in this study are in good agreement with those reported by Kumelan et al.[15,16] around room temperature (difference of about 10%), but the deviation becomes larger at higher temperatures (up to 30% for H_2 and 55% for CO at 373 K). Those authors have determined gas solubility over a large temperature range and for pressures up to about 9 MPa using volumetric measurements on a thermostatted high-pressure cylindrical view cell.

Jacquemin et al.[17] have also investigated the solubility of the two gases as a function of temperature, but near atmospheric pressure, using an isochoric saturation method. The Henry's constants they have reported are systematically lower when compared to the data of this work, with a mean deviation close to 100% both for H_2 and CO.

Berger et al.[10] and Dyson et al.[13] have also measured the solubility of hydrogen in [Bmim][PF$_6$], but only at room temperature. The measurement technique of Berger et al.[10] is similar to the one used in the present work, but in a much lower volume reactor (10 mL of ionic liquid), whereas Dyson et al.[13] have employed high-pressure ^{1}H NMR spectroscopy (at a pressure of 100 atm). According to their results, the numerical values of Henry's constant at room temperature were 5560[10] and 6600 bar[13] which are about 30% and 50% larger than the value obtained in this work, respectively.

Ohlin et al.[14] have reported the solubility of carbon monoxide in several ionic liquids at 295 K using high-pressure ^{13}C NMR spectroscopy. According to these authors the value of Henry's constant in [Bmim] [PF$_6$] at room temperature, 3270 bar, is about 50% higher than in this work.

As said previously, these discrepancies in the data reported by the different authors are probably due to the experimental

techniques applied but maybe also to the impurities present in the samples of ionic liquids used by the different research groups.

4.3. Mass Transfer Studies. 4.3.1. [Bmim][PF$_6$]. 4.3.1.1. Critical Stirrer Speed and Gas Induction. The critical impeller speed N_{cr} at which the onset of gas induction occurs may be considered as the first step in the design of the reactor. Joshi and Sharma[12] have proposed a correlation by measuring the critical impeller speed for pipe and flattened cylindrical impellers and have not found any dependence on liquid property:

$$\frac{N_{cr}^2 d_{st}^2}{gH_l} = \frac{-2}{\pi^2 K} \tag{6}$$

According to the Bernoulli equation and based on the assumption of same velocity for the liquid and the paddle, $K = -1$, whereas the experimental value of K lies in the range of -0.9 to -1.3.

Sawant and Joshi[27] have studied the effect of liquid viscosity (from 0.8 to 80 mPa·s) and found a slight dependence on viscosity, $N_{cr}^2 \propto (\mu/\mu_w)^{0.11}$, resulting in the following equation (which corresponds to $K = -0.97$):

$$\frac{N_{cr}^2 d_{st}^2}{gH_l}\left(\frac{\mu_w}{\mu}\right)^{0.11} = 0.21 \tag{7}$$

More recently Poncin et al.[28] have found a weaker value of the exponent of (μ_w/μ) in eq 7 (0.07).

Due to the large variation of [Bmim][PF$_6$] viscosity in the temperature range, the correlation of Sawant and Joshi[27] was used to calculate the critical stirrer speed, giving 670, 610, and 570 rpm for 293, 323, and 373 K, respectively.

The values calculated previously were found consistent with observations made using a glass beaker of nearly same diameter and heated from the bottom, but it was also seen that gas induction did not proceed the same way at different temperatures (cf. Figure 5). At 293 K, bubbles were not released continuously and most of the gas holdup was trapped around the stirrer blades (Figure 5a) over a large range of stirrer speed, whereas at 373 K gas was dispersed in the whole liquid (Figure 5c) in form of small bubbles above critical speed.

4.3.1.2. Gas−Liquid Mass Transfer. Experiments were carried out to determine the gas−liquid mass transfer coefficient for hydrogen and carbon monoxide in [Bmim][PF$_6$]. They were performed at the same three temperatures, using the dynamic pressure step method discussed in section 3.3.

In Figure 6 the values of the volumetric mass transfer coefficient $k_L a$ are plotted versus the stirrer speed at the three temperatures. Each point is a mean of three to four measurements with standard deviation less than 10%.

$k_L a$ increases with increasing N (rotation speed) and also with temperature. The last effect is much higher than in usual aqueous solutions, probably due to a much higher decrease of viscosity with temperature in ionic liquids and due to the very peculiar change in gas dispersion as shown in Figure 5.

It is usually agreed that mass transfer can be nicely correlated as a function of power consumption.[21,28,29]

An alternative approach when this parameter cannot be evaluated is to describe the effect of different operating parameters on $k_L a$ using a dimensionless correlation of the form $Sh = f(Re, Fr, Sc, We,...)$. The following paragraphs refer to such models.

Dietrich et al.[29] have measured the gas−liquid mass transfer in nonelectrolytic liquids (distilled water, ethanol, and reaction
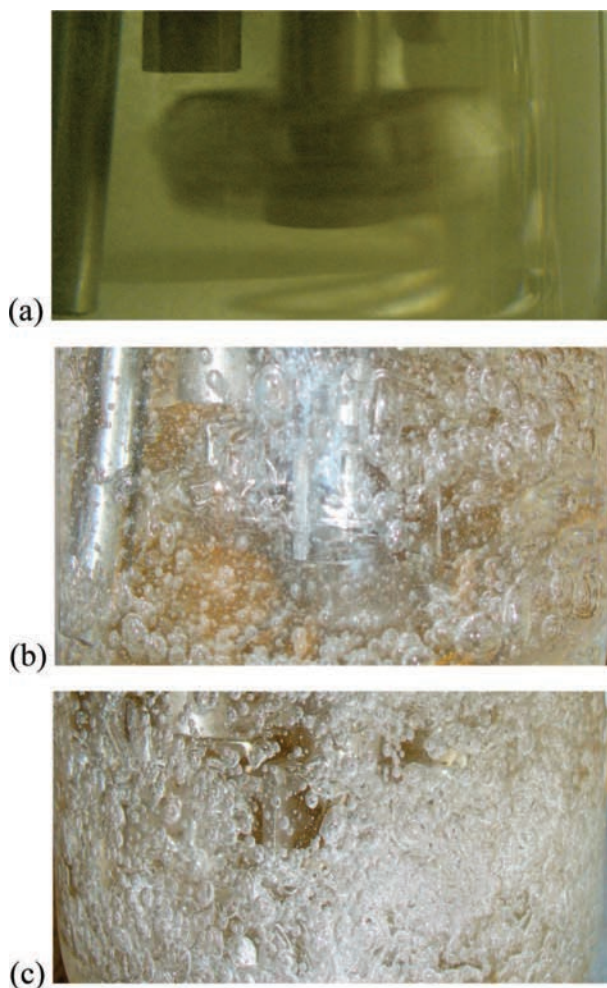
Figure 5. Photographs of the gas dispersion (air) inside [Bmim][PF$_6$] at 1500 rpm: (a) 293 (b) 323, and (c) 373 K.

mixtures involved in adiponitrile hydrogenation) using a gas-inducing stirrer of Rushton type and proposed the following correlation:

$$Sh = 10^a Re^{1.45} Sc^{0.5} We^{0.5} \tag{8}$$

where a was found to be a function of the ratio between liquid height and tank diameter.

As this equation does not account for the critical impeller speed N_{cr}, it will fail near the onset of gas induction, and thus it is only suitable for stirrer speeds $N \gg N_{cr}$.

Poncin et al.[28] have also characterized mass transfer performance of a gas−liquid stirred tank provided with a radial gas-inducing turbine, and they have proposed an empirical correlation for an air−water system:

$$k_L a = 0.065 \frac{(Fr - Fr_{cr})^{1.1}}{1 + 0.132(Fr - Fr_{cr})^{1.1}} \tag{9}$$

This correlation shows that $k_L a$ strongly increases with N above N_{cr}; the asymptotic value at high Fr does not correspond to usual stirring conditions.

Recently Zieverink et al.[21] have studied the gas−liquid mass transfer characteristics of a laboratory autoclave equipped with a gas-inducing Rushton stirrer using different organic liquids (sunflower oil, toluene, acetone, n-hexadecane) with a viscosity range from 0.4 to 60 mPa·s. After evaluating many dimensionless correlations, they have found that $Sh \propto Re^b(Fr - Fr_{cr})^c Sc^d$
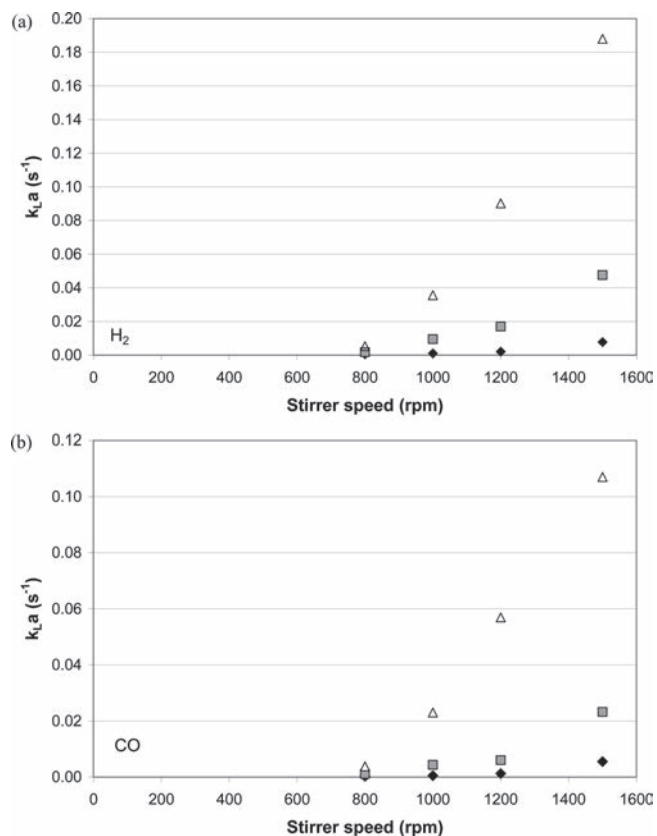
best fitted their data. As the organic liquids used in their study were very similar in surface tension and density, they omitted the Weber number effect.

In the present work, the values of the volumetric gas−liquid mass transfer coefficient $k_L a$ for hydrogen and carbon monoxide in [Bmim][PF$_6$] obtained by dynamic absorption technique were modeled using different correlations based on Sh, Sc, Re, and (or) Fr as relevant dimensionless groups. Previous parametric study indeed underlined the influence of stirrer speed, viscosity (through temperature effect), and gas diffusivity (changing gas nature) on $k_L a$.

All the selected model equations and fitted parameters with 95% confidence interval are listed in Table 4. Those parameters were optimized using Levenberg−Marquardt method (DataFit software) after linearization of the equations. To compare the quality of prediction of the different models, the root-mean-square value between the experimental and predicted $k_L a$ was calculated as

Figure 6. Gas−liquid mass transfer coefficient ($k_L a$) vs stirrer speed (rpm) for H$_2$ (a) and CO (b) in [Bmim][PF$_6$]: 293 (◆), 323 (gray filled square), and 373 K (Δ).

$$rms = \sqrt{\frac{1}{N} \sum_{i=1}^{N} \left(\frac{k_L a_{i,\text{exp}} - k_L a_{i,\text{calc}}}{k_L a_{i,\text{exp}}} \right)^2}$$

Figure 7 presents the parity plots of predicted versus experimental values of mass transfer coefficients. Values at 800 rpm, close to critical speed and maybe too sensitive to any hydrodynamic disturbance, were excluded for the optimization but accounted for in the calculation of the criteria and the plot of parity diagrams.

In accordance with penetration theory models I to IV and VII set the exponent of Schmidt number to 0.5, whereas in equations V and VI it is let free in the fit.

Table 4. Model Equations and Estimated Parameters for Gas−Liquid Mass Transfer with Gas-Inducing Stirrer (with 95% Confidence Intervals)

	model eq	rms[a]	a	b	c	d
I	$Sh = 10^a Re^b Sc^{0.5}$	2.59	$-1.967\,(\pm0.710)$	$1.503\,(\pm0.275)$		
II	$Sh = 10^a (Re - Re_{cr})^b Sc^{0.5}$	0.95	$-1.290\,(\pm0.404)$	$1.415\,(\pm0.177)$		
III	$Sh = 10^a (Re - Re_{cr})^b Fr^c Sc^{0.5}$	0.44	$-1.262\,(\pm0.318)$	$1.354\,(\pm0.145)$	$0.863\,(\pm0.551)$	
IV	$Sh = 10^a Re^b (Fr - Fr_{cr})^c Sc^{0.5}$	0.44	$-1.658\,(\pm0.408)$	$1.388\,(\pm0.157)$	$1.148\,(\pm0.399)$	
V	$Sh = 10^a Re^b Sc^d$	0.95	$-14.012\,(\pm8.154)$	$3.612\,(\pm1.441)$		$1.816\,(\pm0.889)$
VI	$Sh = 10^a (Re - Re_{cr})^b Sc^d$	0.50	$-4.742\,(\pm3.189)$	$2.012\,(\pm0.570)$		$0.919\,(\pm0.384)$
VII	$Sh = 10^a Re^b Sc^{0.5} We^{0.5}$	1.60	$-3.140\,(\pm0.561)$	$1.444\,(\pm0.217)$		

[a] rms is the root-mean-square value between the experimental and predicted $k_L a$, given as $rms = ((1/N)\sum_{i=1}^{N}[(k_L a_{i,exp} - k_L a_{i,calc})/(k_L a_{i,exp})]^2)^{1/2}$.
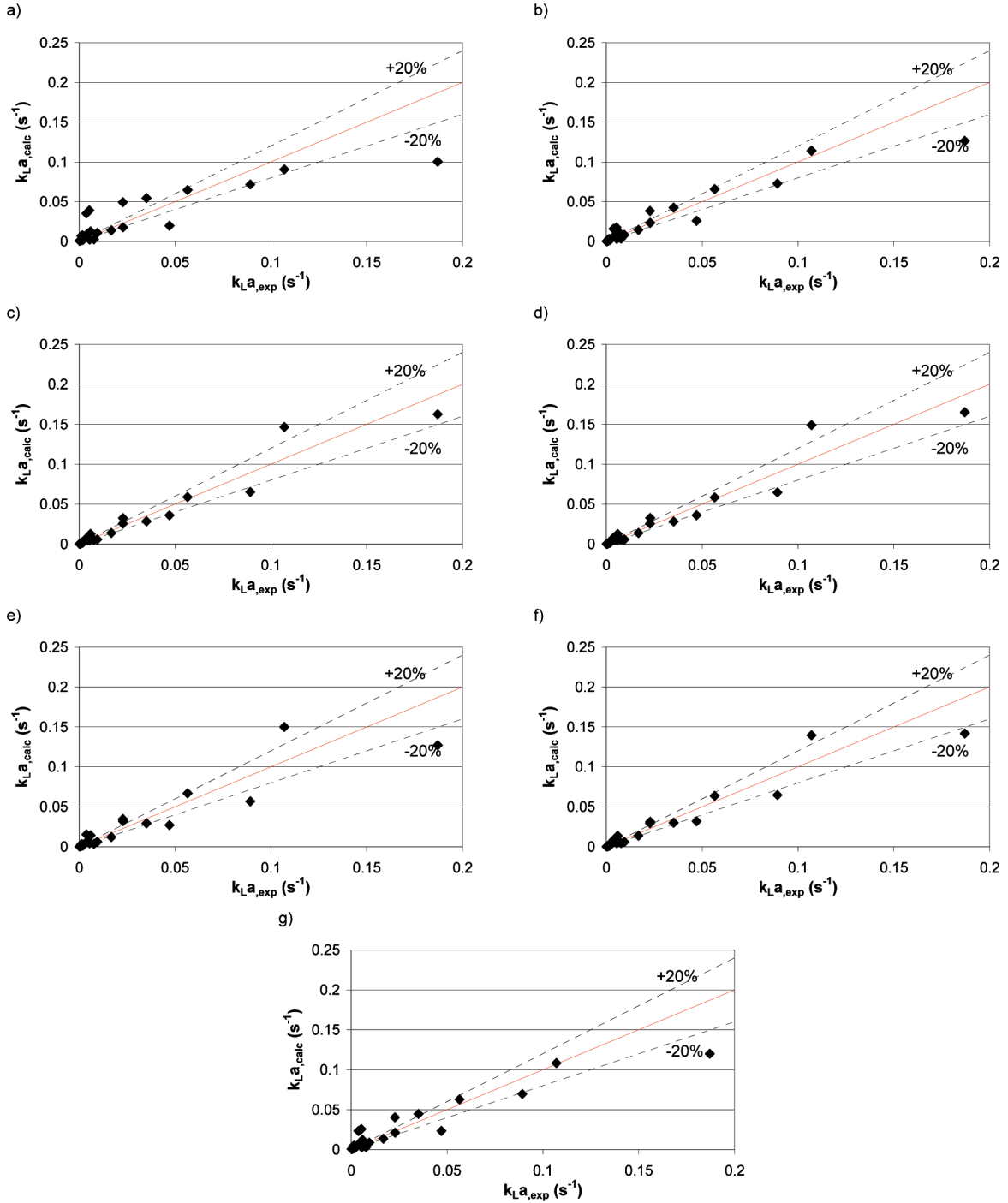

Figure 7. Comparison of calculated vs experimental $k_L a$ for the different model equations listed in Table 4: (a) model I, (b) model II, (c) model III, (d) model IV, (e) model V, (f) model VI, and (g) model VII.

Relations I, V, and VII are based on usual Reynolds number (using the impeller speed N) and exclude critical impeller speed N_{cr} from analysis. Conversely model equations II and VI take into account zero mass transfer when gas induction has not

started by introducing critical impeller speed in critical Reynolds number. The rest of the equations, i.e., III and IV, follows the approach proposed by Zieverink et al.[21] and use a combination of Re and Fr, with one of the two factors corrected for the onset of gas induction. It could be argued that the soundest combination should involve the Reynolds number to account for the actual turbulence in the reactor and a modified Froude number, $Fr - Fr_{cr}$, to account for the induced gas flow rate.

Correlations giving Sh as a function of $Sc^{0.5}$ and Fr^c (or ($Fr - Fr_{cr}$)^c) fail to predict the data over the temperature range as they underestimate the effect of viscosity. Letting the exponent of Sc free results thus for this parameter to negative values which have no physical significance. It was also observed by Zieverink et al.[21] when trying to correlate the k_La values obtained for different liquids.

If in equation III or IV no constraint is put on the Sc exponent, then the optimization leads again to unrealistic negative values for this parameter, along with very large confidence intervals, showing that too many free parameters are involved in fitting our data set.

From analysis of selected models (Table 4), following conclusions can be brought about:

- As expected, taking into account the critical stirrer speed through modified Reynolds number results in much lower rms criteria (0.95 for model II against 2.59 for model I, 0.50 for model VI against 0.95 for model V).
- Letting Sc exponent free in models I and II (resulting in models V and VI, respectively) also decreases rms criteria but also leads to larger confidence intervals due to the huge influence of viscosity on k_La values (μ appears in both Sc and Re numbers).
- Including the Weber number in eq I with a square root dependence, as proposed by Dietrich et al.,[29] allows a better fitting of k_La values, but the criteria is still quite high. As only one ionic liquid was used, variation of surface tension in the operating range is maybe too low to accurately account for this parameter. It should be noted that the fitted exponent of Reynolds (1.44) is in good agreement with what obtained Dietrich et al.[29]
- Models III and IV using a combination of Re and Fr, with one of the two factors corrected for the onset of gas induction, lead to the lowest criteria, and no clear discrimination can be made in between the two models.

4.3.2. [Bmim][PF$_6$]−Decane Mixtures. Finally the gas−liquid mass transfer coefficient was measured in [Bmim][PF$_6$]−decane mixtures at 373 K, using different volume ratios of the two phases, in order to mimic conditions of biphasic hydroformylation.

First it is noteworthy that mass transfer coefficients in ionic liquid phase are about 10 times smaller than in organic phase. As solubility (per volume) is of same order of magnitude this mass transfer limitation may become important even for moderately fast reactions.

In the reaction mixture, k_La increases when increasing decane volume fraction due also to lowering of emulsion viscosity. The larger increase was found around phase inversion (cf. Figure 8). These results are very important as possible industrial reaction will be carried out in such two-liquid-phase media where gas−liquid mass transfer is clearly better than in pure ionic liquid phase due to both the average viscosity reduction and to the very fast liquid−liquid mass transfer as compared to gas−liquid.[8,30] In this two-phase liquid system with ionic liquid as the dispersed phase, gas is fast transferred to the organic phase due to high k_La, then faster transferred to the ionic liquid
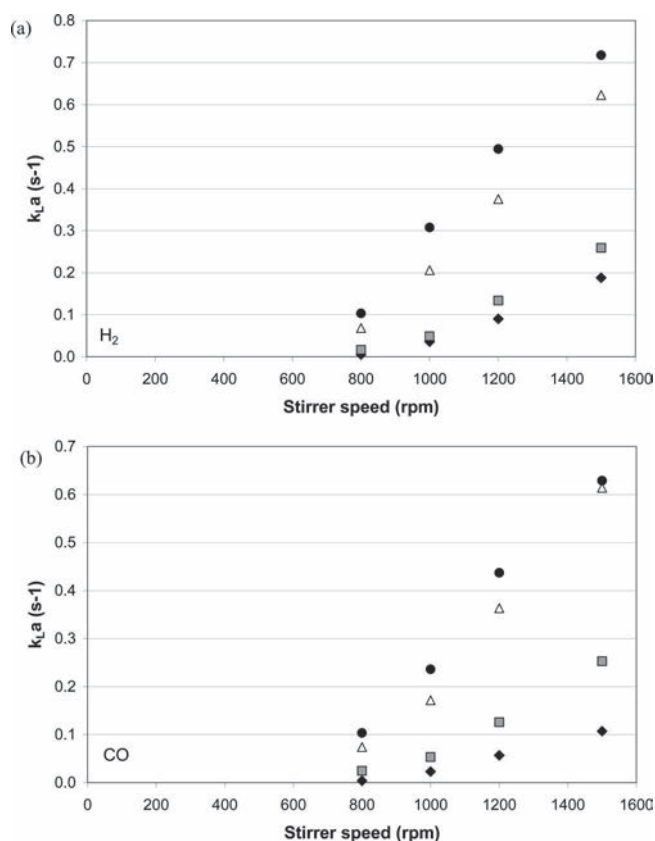

Figure 8. Gas−liquid mass transfer coefficient (k_La) vs stirrer speed (rpm) for H$_2$ (a) and CO (b) in [Bmim][PF$_6$] (◆), decane (●), and [Bmim][PF$_6$]−decane mixtures (0.67/0.33 vol ratio gray filled square; 0.33/0.67 vol ratio Δ) at 373 K.

phase due to much higher interfacial area, droplets being much smaller than gas bubbles.

5. Conclusion

The present work reports experimental results on the solubility of hydrogen and carbon monoxide in [Bmim][PF$_6$] at different temperatures and pressure up to 25 bar. [Bmim][PF$_6$] exhibits low syngas solubility (around 3 times lower than in decane at 373 K) which is not convenient for hydroformylation kinetics. Gas−liquid mass transfer coefficients were also measured in this ionic liquid, showing a very strong effect of both temperature and stirrer speed. Correlations were proposed using various dimensionless parameters including modified Reynolds or Froude numbers to account for the critical impeller speed. Best fit was obtained for models of the form $Sh \propto Re^b(Fr - Fr_{cr})^c Sc^{0.5}$ or $Sh \propto (Re - Re_{cr})^b Fr^c Sc^{0.5}$. In [Bmim][PF$_6$]−decane mixtures, a large increase of k_La was found near phase inversion while increasing decane fraction. Thus, from an engineering point of view, biphasic hydroformylation using ionic liquids should be preferentially conducted with a continuous organic phase in order to reduce the effect of gas−liquid mass transfer limitations.

Nomenclature

d_R = reactor diameter, m
d_{st} = stirrer diameter, m

g = gravitational constant, m·s^{-2}
t = time, s
D = diffusivity of gas in ionic liquid, m^2·s^{-1}
Fr = Froude number, $N^2 d_{st}^2/(gH_l)$, dimensionless
Fr_{cr} = critical Froude number, $N_{cr}^2 d_{st}^2/(gH_l)$, dimensionless
H_l = liquid height above impeller, m
H = Henry's constant, bar
$k_L a$ = volumetric gas−liquid mass transfer coefficient (liquid-phase side), s^{-1}
N = stirrer speed, s^{-1}
N_{cr} = critical stirrer speed, s^{-1}
P = pressure, bar
P_0 = equilibrium pressure after degassing the liquid, bar
P_{atm} = atmospheric pressure, bar
P_m = initial pressure (just before gas absorption), bar
P_f = equilibrium final pressure (after gas absorption), bar
Re = Reynolds number, $\rho N d_{st}^2/\mu$, dimensionless
Re_{cr} = critical Reynolds number, $\rho N_{cr} d_{st}^2/\mu$, dimensionless
Sh = Sherwood number, $k_L a \cdot d_{st}^2/D$, dimensionless
Sc = Schmidt number, $\mu/(\rho D)$, dimensionless
T = temperature, K
W = width of baffle, m
We = Weber number, $\rho N^2 d_{st}^3/\sigma$, dimensionless

Greek Symbols

ρ = density of ionic liquid, kg·m^{-3}
σ = surface tension of ionic liquid, N·m^{-1}
μ = viscosity of ionic liquid, Pa·s
μ_w = viscosity of water, Pa·s

Literature Cited

(1) Chauvin, Y.; Mussmann, L.; Olivier, H. A Novel Class of Versatile Solvents for Two-Phase Catalysis: Hydrogenation, Isomerization, and Hydroformylation of Alkenes Catalyzed by Rhodium Complexes in Liquid 1,3-Dialkylimidazolium Salts. *Angew. Chem., Int. Ed.* **1995**, *34* (23−24), 2698.

(2) Wasserscheid, P.; Keim, W. Ionic Liquids−New "Solutions" for Transition Metal Catalysis. *Angew. Chem., Int. Ed.* **2000**, *39*, 3772.

(3) Wasserscheid, P.; Welton, T. *Ionic Liquids in Synthesis*; Wiley-VCH: Weinheim, Germany, 2003.

(4) Hablot, I.; Jenck, J.; Casamatta, G.; Delmas, H. Gas−Liquid−Liquid Reaction using Water Soluble Catalyst. *Chem. Eng. Sci.* **1992**, *47* (9−11), 2689.

(5) Purwanto, P.; Delmas, H. Gas−Liquid−Liquid Reaction Engineering: Hydroformylation of 1-Octene using a Water Soluble Rhodium Complex Catalyst. *Catal. Today* **1995**, *24* (1−2), 135.

(6) Purwanto, P.; Deshpande, R. M.; Chaudhari, R. V.; Delmas, H. Solubility of Hydrogen, Carbon Monoxide, and 1-Octene in Various Solvents and Solvent Mixtures. *J. Chem. Eng. Data* **1996**, *41*, 1414.

(7) Deshpande, R. M.; Purwanto, P.; Delmas, H.; Chaudhari, R. V. Kinetics of Hydroformylation of 1-Octene Using [Rh(COD)Cl]$_2$−TPPTS Complex Catalyst in a Two-Phase System in the Presence of a Cosolvent. *Ind. Eng. Chem. Res.* **1996**, *35*, 3927.

(8) Lekhal, A.; Chaudhari, R. V.; Wilhelm, A. M.; Delmas, H. Mass Transfer Effects on Hydroformylation Catalyzed by a Water Soluble Complex. *Catal. Today* **1999**, *48* (1−4), 265.

(9) Jauregui-Haza, U. J.; Dessoudeix, M.; Kalck, Ph.; Wilhelm, A. M.; Delmas, H. Multifactorial Analysis in the Study of Hydroformylation of Oct-1-ene Using Supported Aqueous Phase Catalysis. *Catal. Today* **2001**, *66* (2−4), 297.

(10) Berger, A.; de Souza, R. F.; Delgado, M. R.; Dupont, J. Ionic Liquid-Phase Asymmetric Catalytic Hydrogenation: Hydrogen Concentration Effects on Enantioselectivity. *Tetrahedron: Asymmetry* **2001**, *12*, 1825.

(11) Anthony, J. L.; Maginn, E. J.; Brennecke, J. F. Solubilities and Thermodynamic Properties of Gases in the Ionic Liquid 1-*n*-Butyl-3-methylimidazolium Hexafluorophosphate. *J. Phys. Chem. B* **2002**, *106*, 7315.

(12) Joshi, J. B.; Sharma, M. M. Mass Transfer and Hydrodynamic Characteristics of Gas-Inducing Type of Agitated Contactors. *Can. J. Chem. Eng.* **1977**, *55*, 683.

(13) Dyson, P. J.; Laurenczy, G.; Ohlin, C. A.; Vallance, J.; Welton, T. Determination of Hydrogen Concentration in Ionic Liquids and the Effect (or Lack of) on Rates of Hydrogenation. *Chem. Commun.* **2003**, 2418.

(14) Ohlin, C. A.; Dyson, P. J.; Laurenczy, G. Carbon Monoxide Solubility in Ionic Liquids: Determination, Prediction and Relevance to Hydroformylation. *Chem. Commun.* **2004**, 1070.

(15) Kumelan, J.; Perez-Salado Kamps, A.; Tuma, D.; Maurer, G. Solubility of CO in the Ionic Liquid [bmim][PF$_6$]. *Fluid Phase Equilib.* **2005**, *228−229*, 207.

(16) Kumelan, J.; Perez-Salado Kamps, A.; Tuma, D.; Maurer, G. Solubility of H$_2$ in the Ionic Liquid [bmim][PF$_6$]. *J. Chem. Eng. Data* **2006**, *51* (1), 11.

(17) Jacquemin, J.; Husson, P.; Majer, V.; Costa Gomes, M. F. Low-Pressure Solubilities and Thermodynamics of Solvation of Eight Gases in 1-Butyl-3-methylimidazolium Hexafluorophosphate. *Fluid Phase Equilib.* **2006**, *240*, 87.

(18) Teramoto, M.; Tai, S.; Nishii, K.; Teranishi, H. Effects of Pressure on Liquid-Phase Mass Transfer Coefficients. *Chem. Eng. J.* **1974**, *8* (3), 223.

(19) Ledakowicz, S.; Brehm, A.; Oguz, H. Effect of Suspended Inert Solid Particles on Gas−Liquid Mass Transfer in Mechanically Agitated Contactors. *Hung. J. Ind. Chem.* **1985**, *13* (4), 487.

(20) Chaudhari, R. V.; Gholap, R. V.; Emig, G.; Hofmann, H. Gas−Liquid Mass Transfer in "Dead-End" Autoclave Reactor. *Can. J. Chem. Eng.* **1987**, *65*, 744.

(21) Zieverink, M. M. P.; Kreutzer, M. T.; Kapteijn, F.; Moulijn, J. A. Gas−Liquid Mass Transfer in Benchscale Stirred Tanks-Fluid Properties and Critical Impeller Speed for Gas Induction. *Ind. Eng. Chem. Res.* **2006**, *45*, 4574.

(22) Dzyuba, S. V.; Bartsch, R. A. Influence of Structural Variations in 1-Alkyl(aralkyl)-3-methylimidazolim Hexafluorophosphates and Bis(trifluoromethylsulfonyl)imides on Physical Properties of the Ionic Liquids. *ChemPhysChem* **2002**, *3*, 161.

(23) Huddleston, J. G.; Visser, A. E.; Reichert, W. M.; Willauer, H. D.; Broker, G. A.; Rogers, R. D. Characterization and Comparison of Hydrophilic and Hydrophobic Room Temperature Ionic Liquids Incorporating the Imidazolium Cation. *Green Chem.* **2001**, *3*, 156.

(24) Fadeev, A. G.; Meagher, M. M. Opportunities for Ionic Liquids in Recovery of Biofuels. *Chem. Commun.* **2001**, 295.

(25) Baker, S. N.; Baker, G. A.; Kane, M. A.; Bright, F. V. The Cybotactic Region Surrounding Fluorescent Probes Dissolved in 1-Butyl-3-methylimidazolium Hexafluorophosphate: Effects of Temperature and Added Carbon Dioxide. *J. Phys. Chem. B* **2001**, *105* (39), 9663.

(26) Morgan, D.; Ferguson, L.; Scovazzo, P. Diffusivities of Gases in Room-Temperature Ionic Liquids: Data and Correlations Obtained Using a Lag-Time Technique. *Ind. Eng. Chem. Res.* **2005**, *44*, 4815.

(27) Sawant, S. B.; Joshi, J. B. Critical Impeller Speed for the Onset of Gas Induction in Gas-Inducing Types of Agitated Contactors. *Chem. Eng. J.* **1979**, *18*, 87.

(28) Poncin, S.; Nguyen, C.; Midoux, N.; Breysse, J. Hydrodynamics and Volumetric Gas−Liquid Mass Transfer Coefficient of a Stirred Vessel Equipped with a Gas-Inducing Impeller. *Chem. Eng. Sci.* **2002**, *57*, 3299.

(29) Dietrich, E.; Mathieu, C.; Delmas, H.; Jenck, J. Raney-Nickel Catalyzed Hydrogenations: Gas−Liquid Mass Transfer in Gas-Induced Stirred Slurry Reactors. *Chem. Eng. Sci.* **1992**, *47* (13−14), 3597.

(30) Dumont, E.; Delmas, H. Mass Transfer Enhancement of Gas Absorption in Oil-in-Water Systems: A Review. *Chem. Eng. Process.* **2003**, *42* (6), 419.